Chapter 2

Studies on the Langmuir monolayers of cholesteryl derivatives

2.1 Introduction

Cholesteryl esters are biologically important. They are found concentrated in the interior lipid core of chylomicrons and in apolipoproteins [1, 2]. These cholesteryl esters are also found in atherosclerotic lesions [3]. The higher homologue of esters take part in hydrolysis and are responsible in transport of free cholesterol [4]. Some of the cholesteryl esters are also mesogenic.

The monolayers of sterol and short chain cholesteryl esters have been studied with emphasis on the nucleation and crystallization process at the air-water(A-W) interface [5] and on the inhibition of crystallization of these sterols with lipids [6]. Short chain derivatives of cholesteryl esters like formate and acetate yield stable monolayers [7]. The higher homologue of cholesteryl esters were found to form unstable monolayer at the A-W interface [8]. However, for some other cholesteryl derivatives there has not been a study of the monolayer properties at the A-W interface.

In this chapter, we describe our systematic investigations on the monolayer phases, structure and aggregation of the films of cholesteryl derivatives at the A-W interface.

2.2 Experiment

In our studies we used the following compounds: They were 1.) cholesterol(Ch), 2.) cholesteryl acetate(ChA), 3.) cholesteryl heptanoate(ChH), 4.) cholesteryl octanoate(ChO), 5.) cholesteryl nonanoate(ChN), 6.) cholesteryl laurate(ChL), 7.) cholesteryl myristate(ChM), 8.) cholesteryl palmitate(ChP), 9.) cholesteryl stearate(ChS), 10.) cholesteryl benzoate(ChB), 11.) cholesteryl hydro cinnamate(ChHC), 12.) cholesteryl oleate(ChOl) and 13.) cholesteryl oleyl carbonate(ChOC). These were obtained from Sigma and Aldrich. The materials, Ch, ChA, ChH, ChO, ChN, ChL, ChM, ChS, ChP, ChB and ChHC have been recrystallized twice and the purity of them were checked by thin layer chromatography technique and the melting point was checked using Mettler hot stage. The materials ChOl and ChOC were used as procured.

A solution of concentration, 1mg:1ml, was prepared using chloroform(HPLC grade) as a solvent. The surface manometry experiments were carried out using Nima 611M trough. The subphase used was Millipore Milli-Q water with a pH of about 5.7. The relative humidity was around 85±5%. Small drops of solution were spread all over the trough between the barriers using a microsyringe(Hamilton). The system was equilibrated for 10 minutes allowing the solvent to evaporate. The entire trough was enclosed inside an Perspex glass box to prevent contaminants, air drag and to minimize evaporation. The surface pressure(π) was measured using the standard Wilhelmy plate technique using a filter paper. The details are given in chapter-1. The A/M was obtained by symmetric compression of the barriers. The isotherm data were subjected to a running average of 10 data points. All the experiments were done at room temperature(t) of 25±1°C and the monolayers were compressed at 4cm^2/min.

Equilibrium spreading pressure(ESP) was measured at constant area of 100 cm^2. Here 0.01mg of finely grounded crystals were added to the subphase at room temperature. High humidity of the order of 92±5% was maintained during the experiment to prevent any evaporation. The duration of these experiments were varied from a few hours to a day.

Epifluorescence microscopy [9, 10] was used to characterize the phases indicated by

the $\pi - A/M$ studies. A fluorescent dye 4-(hexadecylamino)-7-nitrobenz-2 oxa-1,3 diazole (NBDHDA) was obtained from Molecular Probes. About 1% molar concentration was added as a dopant to the solution. The monolayer was directly observed under a Leitz Metalux 3 microscope. The images were obtained using a photon intensified CCD camera(Model P 46036A/V22, EEV). The surface topography of the thicker domains were studied by reflection microscopy and the images were taken using a Sony CCD(DXC-390P) camera. The details are given in chapter-1.

Brewster angle microscopy(BAM) [11, 12] was used to observe the monolayers of cholesteryl derivatives at the A-W interface. The advantage of this technique over epifluorescence microscopy was that a dye was not required. The MiniBAM(NFT, Nanotech, Germany) was the BAM microscope used for our imaging. A p-polarized laser beam of wavelength 660 *nm* with a power of 30 mW strikes the subphase at Brewster angle(53°). The reflected light from the monolayer covered interface was sensed by a detector. This detector output(composite signal) was connected to the frame grabber(PCI 1401 - National Instruments) with a capture rate of 25 frames/sec. The field of view for all the BAM images is 6.4 x 4.8 mm^2. Another advantage of using the BAM technique in combination with epifluorescence was to get the textures with different spatial length scale.

2.3 Results

The π- A/M isotherm of Ch derivatives are shown in the Figure 2.1. The monolayer of Ch exhibited a surface pressure less than 0.1 mN/m above an A/M of 40 $Å^2$. This is shown in Figure 2.1(a). The onset of condensed phase was observed with sharp and steep slope change. Limiting area per molecule(A_0) was obtained by extrapolating the linear part of the isotherm to zero surface pressure at the point of collapse. For Ch, the A_0 value was 38.8 $Å^2$ and the collapse pressure was 43.5 mN/m. In literature, the reported values of A_0 ranges from 38 $Å^2$ [13] to 39 $Å^2$ [14]. and the collapse pressures ranges from 52.5 mN/m [14] to 43 mN/m [15]. After the collapse, the isotherm showed a plateau region up to an A/M of 16 $Å^2$. Thereafter, the surface pressure increased sharply. When the compression was

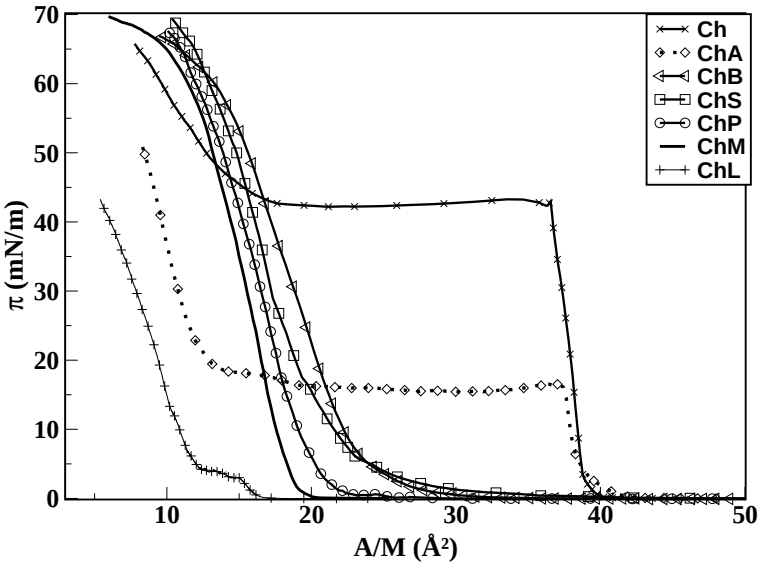

(a)

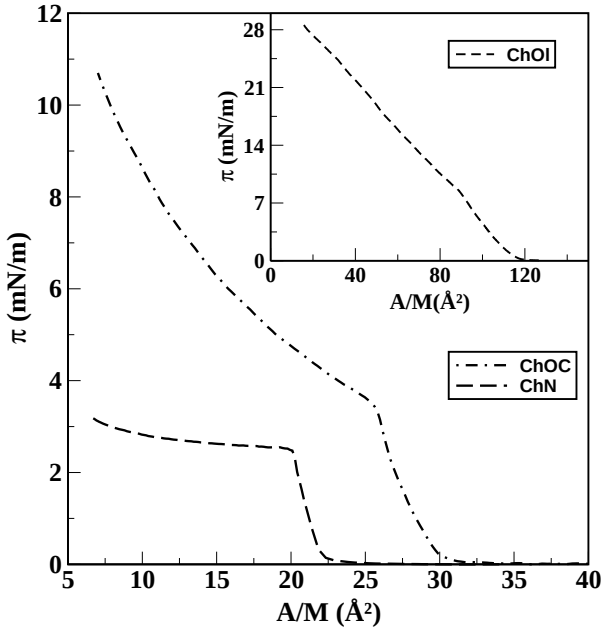

(b)

Figure 2.1: Surface pressure(π) - area per molecule(A/M) isotherms of cholesteryl derivatives at the air-water interface at a temperature, t=25 °C. Figure(a) shows the π-A/M isotherms for cholesterol(Ch), cholesteryl acetate(ChA), cholesteryl benzoate(ChB), cholesteryl stearate(ChS), cholesteryl palmitate(ChP) and cholesteryl myristate(ChM) and cholesteryl laurate(ChL). Figure(b) shows the π-A/M isotherms for cholesteryl oleyl carbonate(ChOC) and cholesteryl nonanoate(ChN). The inset in Figure(b) shows the π-A/M isotherm for cholesteryl oleate(ChOl).

stopped at this region the surface pressure dropped to a value of 40 mN/m. These values were in agreement with the reported values [16]. Cholesteryl acetate isotherm(Figure 2.1(a)) also had similar trend as that of Ch. Upon compression, there was a sharp increase in the surface pressure around 41 $Å^2$. This was followed by a collapse at 15.6 mN/m. For ChA, the A_0 value at collapse was close to that of Ch. Below 19 $Å^2$, the surface pressure increased gradually with compression. The seventh homologue, cholesteryl heptanoate and the eighth homologue cholesteryl octanoate did not form stable monolayers at the A-W interface. The π-A/M isotherm for cholesteryl nonanoate is shown in Figure 2.1(b). The compression of the monolayer led to a rise in the surface pressure around 22.5 $Å^2$. This was followed by a collapse at a surface pressure of 2.2 mN/m with A_0 value of 22 $Å^2$. After the collapse there was a marginal rise in the surface pressure. The isotherm for cholesteryl laurate is shown in Figure 2.1(a). The surface pressure was almost zero above 17.3 $Å^2$. Upon compression, there was an increase in the surface pressure around 17.3 $Å^2$. Upon further compression, the isotherm yielded an A_0 value of 16.7 $Å^2$ and a collapse pressure of 2.6 mN/m. After the collapse, there was a rough plateau region and the surface pressure increased rapidly to a value of about 45 mN/m at 13.1 $Å^2$. Cholesteryl myristate has a long alkyl chain. The π-A/M isotherm yielded an A_0 value of 19.6 $Å^2$ (Figure 2.1(a)). The ChM film was quite stiff at the A-W interface. When the molecules are spread at the A-W interface one can visually observe the micro-crystallites immediately after spreading at a concentration of 1mg:1ml. At high A/M, the isotherm had jitters due to the presence of micro-crystallites which gave rise to the jerky motion. The isotherm showed a steep rise in the surface pressure around 20 $Å^2$. The π value was quite large at low A/M and it rapidly drops on stopping the compression. The trend of the isotherm for ChP(Figure 2.1(a)) was similar to that of ChM. For ChP, A_0 value was found to be 20.7 $Å^2$. The isotherm of ChS(Figure 2.1(a)) also resembled that of ChP. For ChS, A_0 value was found to be 21.4 $Å^2$. In ChM, ChP and ChS the collapse pressures were nearly the same and was around 65 mN/m. The isotherm of ChB(Figure 2.1(a)) showed an increase in π around 30 $Å^2$. Then it started to rise rapidly and collapsed at a value of about 65 mN/m. The trend of the isotherm was similar to the case of higher homologues of cholesteryl

esters but with slightly higher A_0(23.7 Å^2). For ChB, this value of A_0 was almost half of the molecular cross-section which is around 48 Å^2. Cholesteryl hydro cinnamate gave rise to irreproducible isotherms. Cholesteryl Oleate, an unsaturated ester with a bent alkyl chain, gave rise to a stable isotherm(shown as inset in Figure 2.1(b)). On compressing, there was a slope change at 118 Å^2 and the monolayer collapsed with an A_0 value of 114.3 Å^2. The collapse pressure was 8 mN/m. The surface pressure gradually increased after collapse. The isotherm for ChOC(Figure 2.1(b)), which is a room temperature cholesteric, showed a slope change at an A/M of 31 Å^2. The monolayer collapsed at a surface pressure of 3.4 mN/m with A_0 value of 30 Å^2. Thereafter the surface pressure increased gradually.

Equilibrium spreading pressure is the surface pressure at which the monolayer coexists with its bulk phase. Figure 2.2 shows the ESP of Ch and ChA which were around 38.9 mN/m and 7.0 mN/m. For Ch, the ESP was attained with a span of 10 minutes. For ChA, the

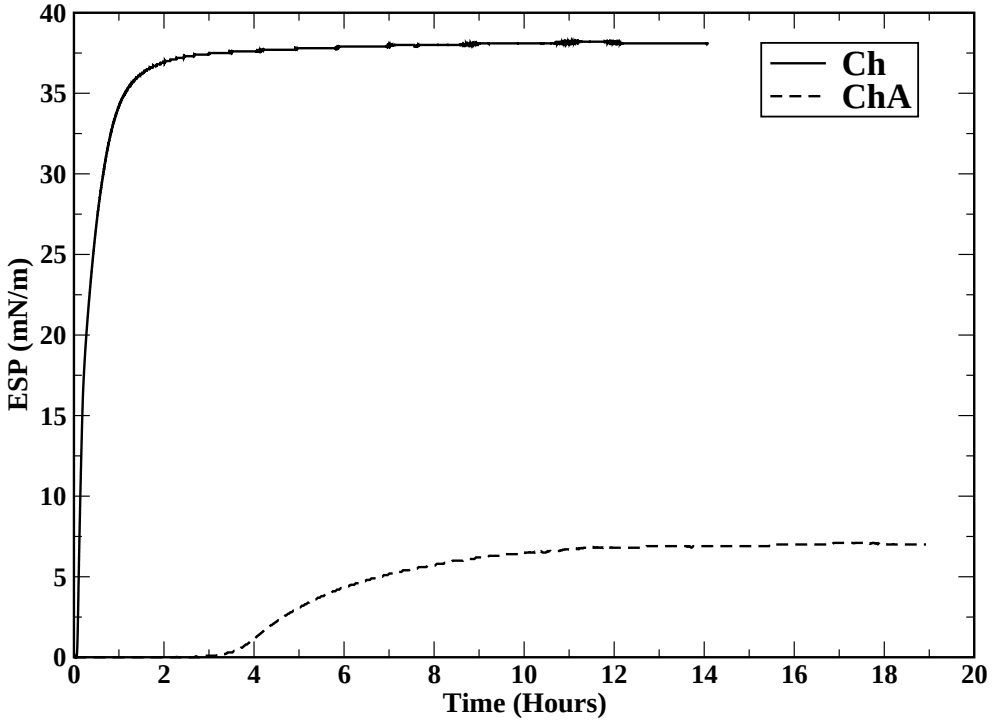

Figure 2.2: Equilibrium spreading pressure(ESP) for Cholesterol(Ch) and Cholesteryl acetate(ChA). The kinetics in attaining the ESP for Ch and ChA are markedly different.

kinetics of monolayer eluting out from the crystallites was very slow. The other compounds like ChB, ChH, ChO, ChM, ChS and ChP did not show any ESP even after waiting for a day.

We have carried out epifluorescence microscopy studies on these derivatives of cholesterol. The epifluorescence textures for Ch are shown in Figure 2.3. The presence of gas(G) +

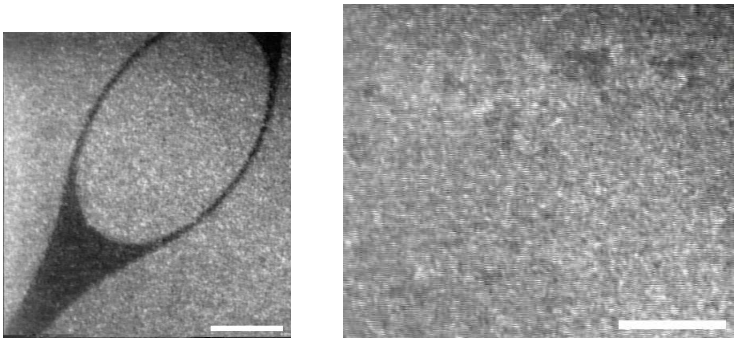

(a) 50.3 Å^2 (b) 34.4 Å^2

Figure 2.3: Epifluorescence images of cholesterol. Figure(a) shows the epifluorescence image for cholesterol exhibiting G + L_2 phase coexistence. Here the dark region represents the gas phase and the grey background represent the L_2 phase. Figure(b) shows the collapsed state. Here, the L_2 phase(grey) and the crystallites(dark) coexist. Scale bar represents 50 μm.

L_2 phase(we represent, the condensed phase as L_2 where the fluorescent dye appeared less bright and less fluid) is shown in Figure 2.3(a). Figure 2.3(b) shows the collapsed state in which the L_2 phase and the Ch crystallites(dark) coexists.

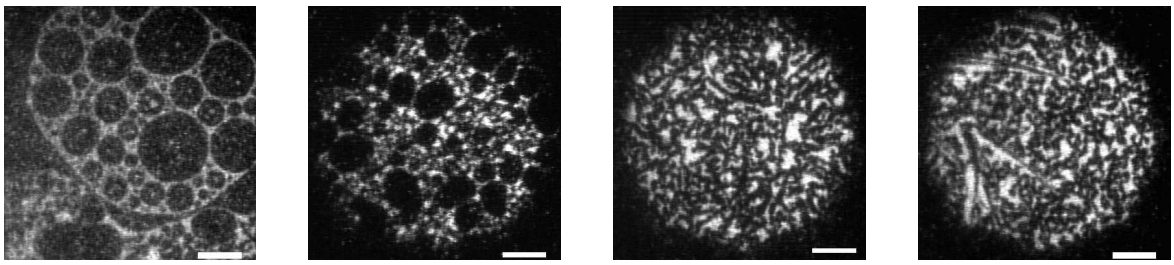

(a) 141.7 Å^2 (b) 128.1 Å^2 (c) 56.2 Å^2 (d) 36.6 Å^2

Figure 2.4: Epifluorescence images of cholesteryl acetate. Figure(a) represents the circular gas(dark) domains coexisting with L_2 phase. Figure(b) represents the diminishing gas(dark) domains upon compression with background being L_2 phase. Figure(c) represents the L_2 phase which appears as meshy network. This is also seen partly in Figures (a) and (b). Figure(d) shows the collapsed ChA crystallites coexisting with L_2 phase. Scale bar represents 50 μm.

In the case of ChA, the textures were very much different from that of Ch under epifluorescence microscope. Epifluorescence images of ChA are shown in Figure 2.4. At very

large A/M of 141.7 Å^2, we could observe the usual circular G domains which appeared dark coexisting with L_2 phase having mesh like texture (Figure 2.4(a)). On compression, the G domains diminished in size as shown in Figure 2.4(b) giving rise to L_2 phase. These L_2 domains possessed irregular boundary and was less fluid(Figure 2.4(c)). These observations indicate the crystalline nature of the monolayer phase. At the collapsed state, the three dimensional(3D) crystallites of ChA were seen to coexist with L_2 phase(mesh texture). This is shown in Figure 2.4(d).

For the seventh homologue ChH and the eighth homologue ChO there was no indication of the usual G and L_2 monolayer phases. Even at larger A/M the epifluorescence images showed a spontaneous formation of 3D crystallites on spreading. Epifluorescence microscopy studies on ChN reveal interesting features as depicted in Figure 2.5. Figure 2.5(a)

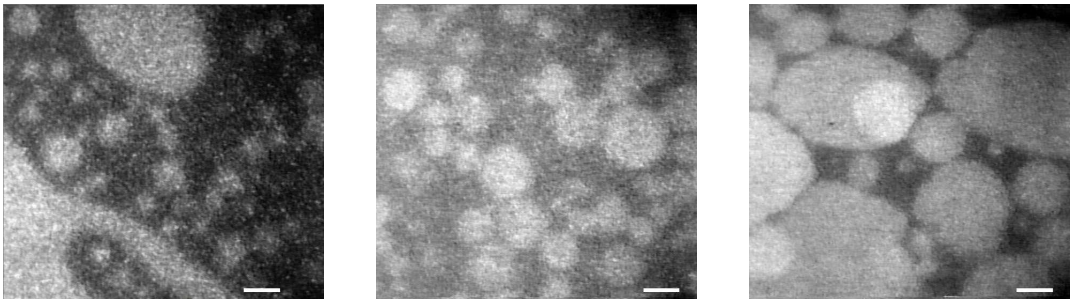

(a) 43.7 Å^2 (b) 21.5 Å^2 (c) 11.0 Å^2

Figure 2.5: Cholesteryl nonanoate images under epifluorescence microscope. Figure(a) shows the coexistence of gas(dark) + bilayer(bright) phase. Figure(b) shows the collapsed state. Here the presence of 3D domains are seen to coexist with background bilayer phase. Figure(c) shows the collapsed state at a very low A/M. Here still thicker domain nucleate(more bright) inside the 3D domain. These 3D domains were in metastable state. Scale bar represents 50 μm.

represents the coexisting G and bilayer domains. This was followed by a transition to an uniform bilayer phase. Based on the A_0 value for ChN, we infer that the condensed phase as a bilayer phase. The bilayer phase was more fluid. In the collapsed state, At still lower A/M, bright circular domains were seen to coexist with bilayer phase(Figure 2.5(b)). At still lower A/M, domains of different intensities were seen(Figure 2.5(c)). At this state, we could see the nucleation and growth of still brighter domains. Upon further compression these domains

grow in size and get distorted from the circular shape. Epifluorescence images for ChL are shown in Figure 2.6. At large A/M, the coexisting G(dark) + bilayer(bright) domains were seen(Figure 2.6(a)). Here, the G(dark) domains appeared to have foam like textures. The bi-

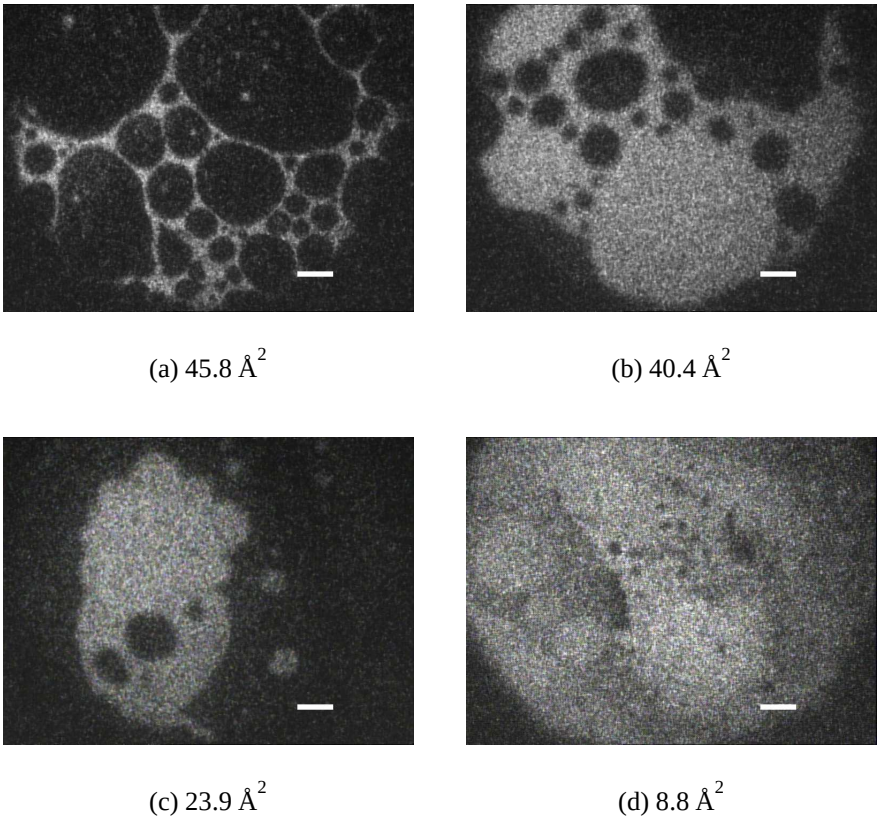

(a) 45.8 $Å^2$ (b) 40.4 $Å^2$

(c) 23.9 $Å^2$ (d) 8.8 $Å^2$

Figure 2.6: Cholesteryl Laurate images under epifluorescence microscope. Figure(a) shows the presence of gas(dark) + bilayer(bright) domains. The bilayer domains are more fluidic. Figure(b) shows the coexistence of bilayer domains with circular and brighter domains with gas(G) phase as background. Figure(c) shows the nucleation and growth of brighter domains with vanishing bilayer. Here the brighter domains get distorted. Figure(d) shows the coexistence of more such bright domains. Scale bar represents 50 μm.

layer domains are more fluidic. At low A/M, brighter circular domains of varying intensities were seen to nucleate from the bilayer domains and coexists with G phase. This is shown in Figure 2.6(b). The brighter domains were more dense when compared to the bilayer domains and were metastable in nature. At still lower A/M, these brighter domains distort from its circular shape and grow at the expense of bilayer phase. This is shown in Figure 2.6(c). Further compression, leads to the growth of these distorted domains(Figure 2.6(d)).

Epifluorescence images for ChM are shown in Figure 2.7. In ChM, we find flakes

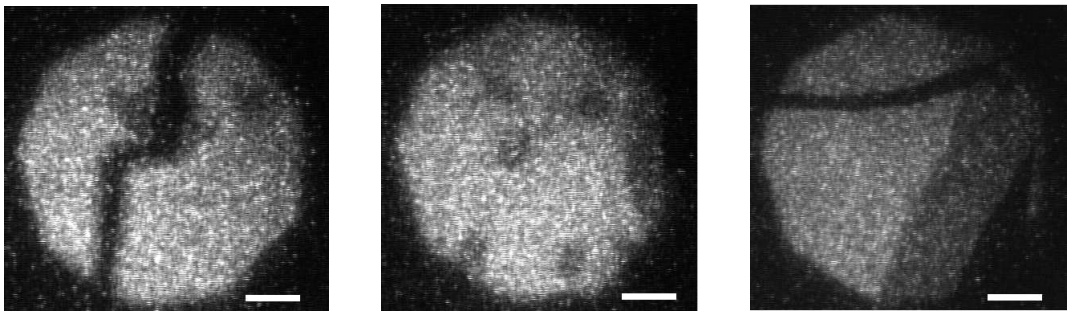

(a) 99.4 Å^2 (b) 81.8 Å^2 (c) 28.0 Å^2

Figure 2.7: Cholesteryl myristate images under epifluorescence microscope. Figure(a) shows the presence of thick flakes with voids. In Figure(b), the presence of dark regions are seen over these flakes. Figure(c) shows the presence of layers with varying intensity revealing the difference in thickness in the flakes. Scale bar represents 50 μm.

with fractured edges even at very large A/M(Figure 2.7(a)). At lower A/M, dark patches were visible on these flakes(Figure 2.7(b)). These flakes were also found to possess varying intensity(Figure 2.7(c)). The textures of ChM and ChP were similar under epifluorescence(Figure 2.8). The epifluorescence studies were also carried out on the films of ChM

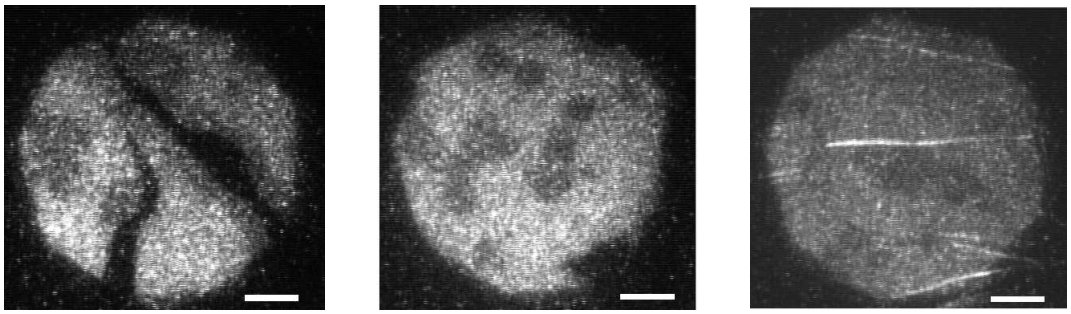

(a) 85.6 Å^2 (b) 52.1 Å^2 (c) 15.1 Å^2

Figure 2.8: Cholesteryl palmitate images under epifluorescence microscope. Figure(a) shows the presence of flakes with voids. Figure(b) shows the presence of dark regions on top of these flakes. In Figure(c), bright streaks can be seen on these flakes. Scale bar represents 50 μm.

and ChS at very low concentration(0.1 mM solution) and at very high A/M of 500 Å^2. Even here the usual G + L_1 phase was absent and the pattern showed the coexistence of flakes with voids. The epifluorescence images for ChS are shown in Figure 2.9. The textures showed

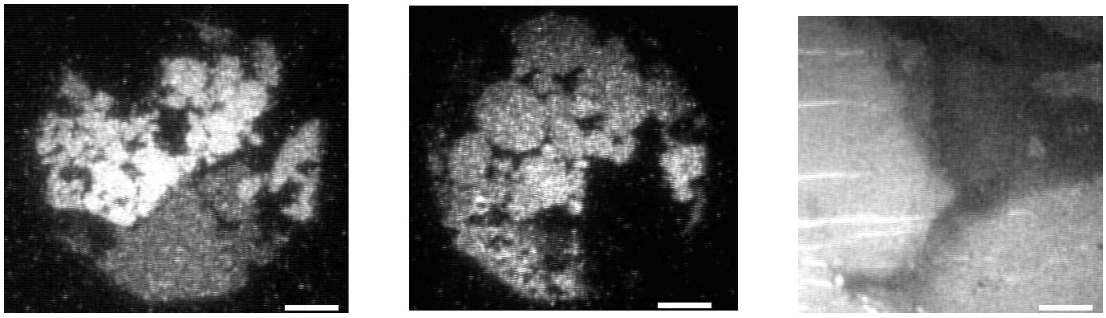

(a) 90.1 Å^2 (b) 42.9 Å^2 (c) 11.8 Å^2

Figure 2.9: Cholesteryl stearate images under epifluorescence microscope. Figures (a) and (b) represent the circular and elongated domains of varying intensity. Figure(c) shows the formation of bright streaks over the domains indicating the crumpling of the domains at low A/M. Scale bar represents 50 μm.

circular and elongated domains(Figure 2.9(a)). These domains possessed different intensities(Figures 2.9(a) and 2.9(b)). Further compression leads to the formation of bright streaks over these domains as shown in Figure 2.9(c). We have undertaken the epifluorescence studies at lower concentration(0.1 mM solution) and at very high A/M. Even here the coexistence of distorted circles with voids were seen and the usual G phase was absent.

The epifluorescence images for ChB are shown in Figure 2.10. ChB exhibits dark and

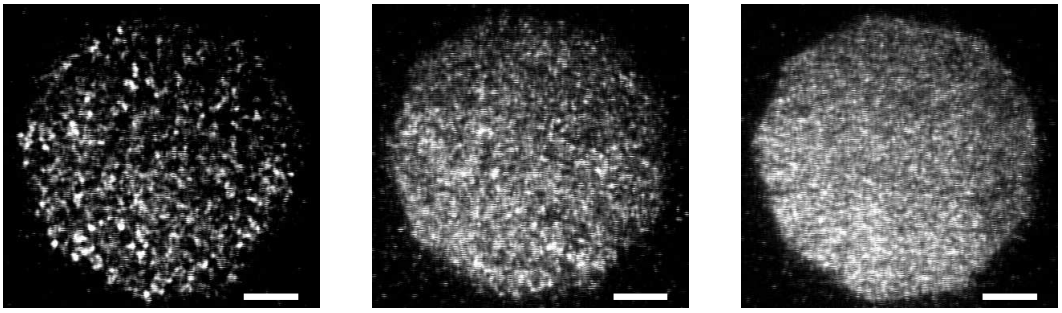

(a) 70.8 Å^2 (b) 38.6 Å^2 (c) 19.6 Å^2

Figure 2.10: Cholesteryl benzoate images under epifluorescence microscope. Figure(a) shows the presence of dark and white domains. These possess less fluidity. Figures (b) and (c) show the occurrence of more and more brighter regions. Scale bar represents 50 μm.

bright domains(Figure 2.10(a)). The dispersion of the fluorescent dye was not good in this system. The film possessed less fluidity indicating the presence of high crystallinity.

Cholesteryl hydro cinnamate was found to form crystallites even at very high A/M. Epifluorescence microscopy on cholesteryl oleate show the usual G + L_1 phase above 120 Å^2. The monolayer exhibits the L_1 phase in the range 118 Å^2 to 90 Å^2 below which it collapses. Figure(2.11) shows the textures in the collapsed state. Immediately after the collapse, the

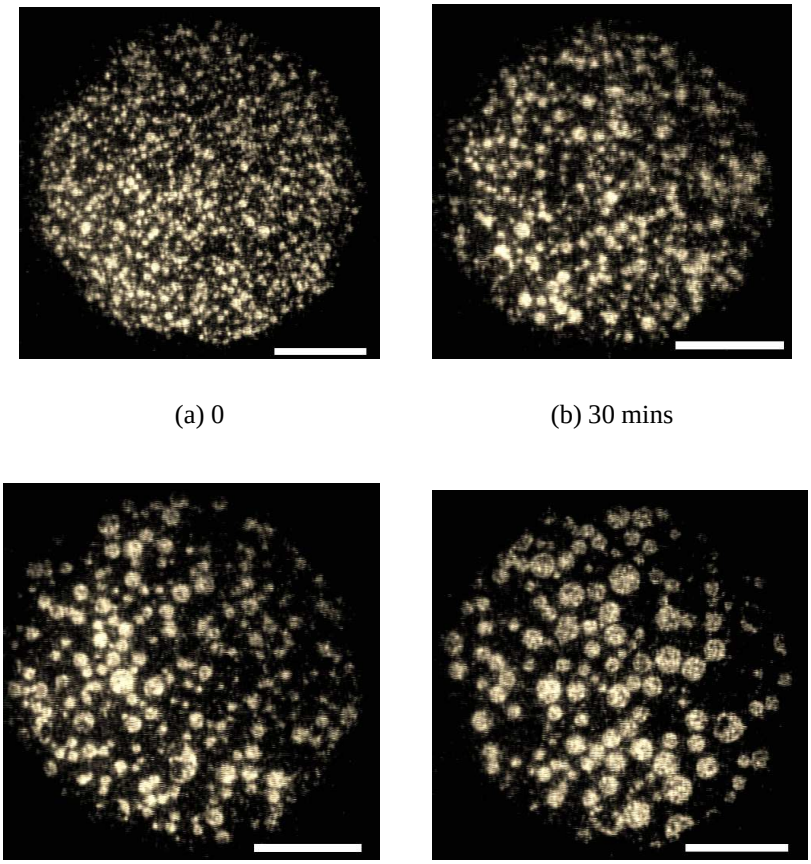

(a) 0 (b) 30 mins

(c) 2 hour (d) 5 hour

Figure 2.11: Epifluorescence images of cholesteryl oleate domains at an A/M of 80 Å^2 showing them evolving in time in the collapsed state. Figure(a) shows the dense texture immediately after the collapse. Figure(b) shows the transformation of these dense texture to small circular domains. Figures (c) and (d) show the evolution of the circular 3D domains to bigger circles. Scale bar represents 50 μm.

presence of dense textures were seen evolving as a function of time (Figure 2.11(a)). The dense textures transform to bright domains. These bright domains grow to bigger circles in time(Figures 2.11(b) to 2.11(d)). Cholesteryl oleyl carbonate under epifluorescence microscope showed the occurrence of G + L_1 + bilayer phase coexistence. The coexistence of G

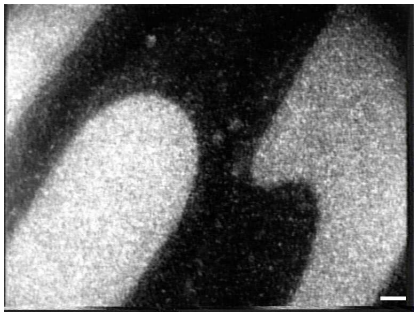

(a) 38 Å^2

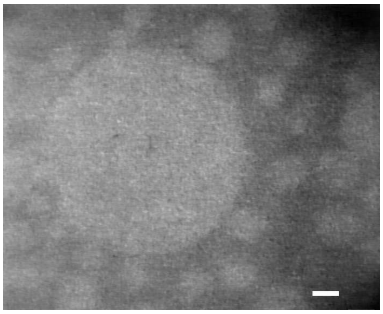

(b) 36 Å^2

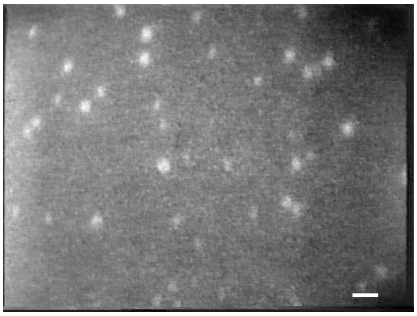

(c) 20.1 Å^2

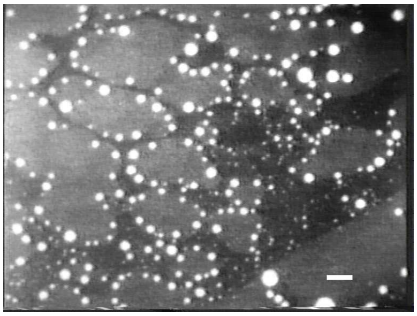

(d) 15.2 Å^2

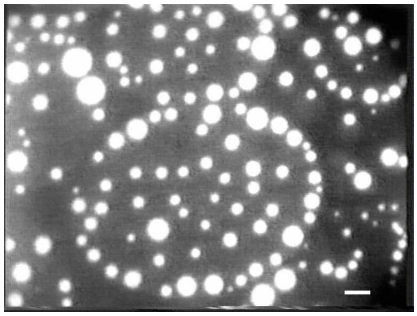

(e) 11.3 Å^2

Figure 2.12: Cholesteryl oleyl carbonate images under epifluorescence microscope. In figure(a), the coexisting G(dark) + L_1(bright) phase is seen. Figure(b) shows the more bright bilayer domains which coexist with L_1 phase in the background. Figure(c) shows the collapsed state. Here, bright 3D spots coexist with bilayer phase in the background. These spots transform to circles. Figure(d) shows the varying intensity(grey) domains coexisting with bright spots. Figure(e) shows the grey domains of slightly different intensities coexisting with very bright 3D circular domains. These 3D circular domains mostly exist at the periphery of the grey domains. Scale bar represents 50 μm.

+ L_1 phase is shown in Figure 2.12(a). The coexistence of L_1 + bilayer phase is shown in Figure 2.12(b). These coexisting phases were seen at low pressures(less than 0.1 mN/m).

After the collapse, small bright 3D spots coexist with bilayer phase(Figure 2.12(c)). These bright spots which were initially small transform to circles. Their number also increases on decreasing the A/M. These bright circular domains were found to arrange themselves at the periphery of the grey domains(Figures 2.12(d) and 2.12(e)).

Brewster angle microscopy was employed to confirm the monolayer phases seen under epifluorescence microscope. For the case of Ch, the BAM images are shown in Figure 2.13. Figure 2.13(a) shows the coexisting G + L_2 phase. With compression, the presence of L_2

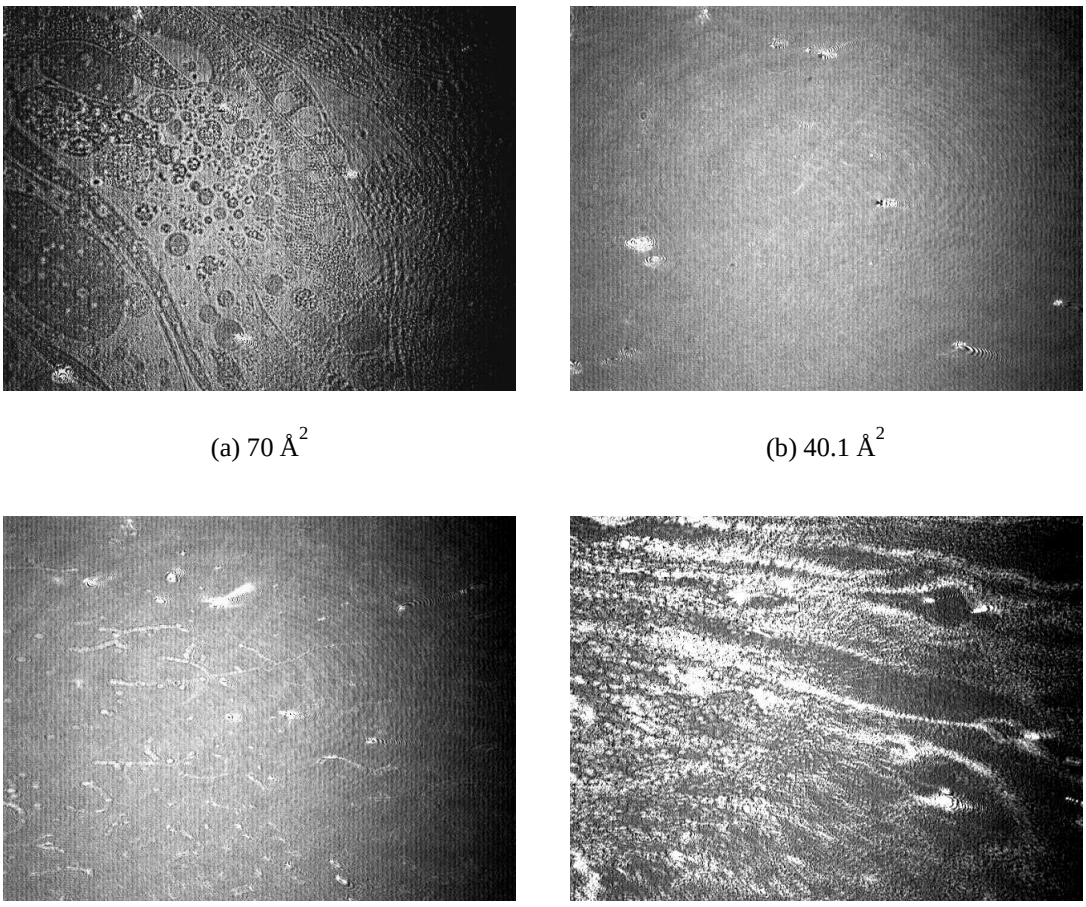

(a) 70 Å^2 (b) 40.1 Å^2

(c) 30.7 Å^2 (d) 18.5 Å^2

Figure 2.13: Brewster angle microscopy images of cholesterol. Figure(a) shows the coexistence of gas + L_2 domains. Figure(b) shows the predominantly present L_2 phase. Figure(c) shows the collapsed state. The texture shows the coexistence of crystallites(streaks) with L_2 phase(background). Figure(d) shows the nucleation and growth of the crystallites. Each image has the dimension of 6.4 x 4.8 mm^2.

phase was seen(Figure 2.13(b)). After the collapse, bright 3D crystals(streaks) nucleate from

the L_2 phase (Figure 2.13(c)) and grow into crystallites(Figure 2.13(d)). BAM images for ChA are shown in Figure 2.14. The presence of L_2 phase with well defined boundaries

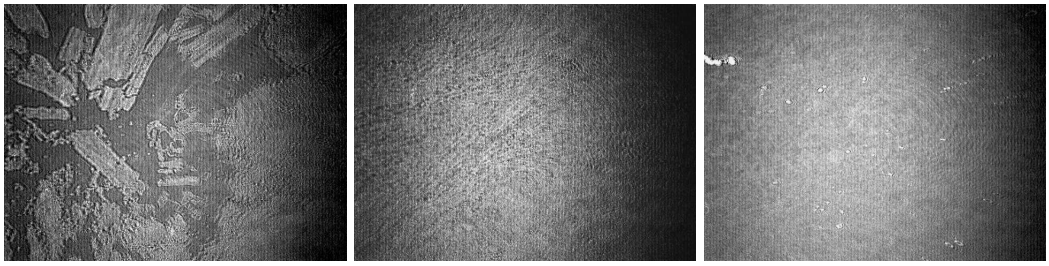

(a) A/M=186.3 Å^2 (b) A/M=70.1 Å^2 (c) A/M=40.3 Å^2

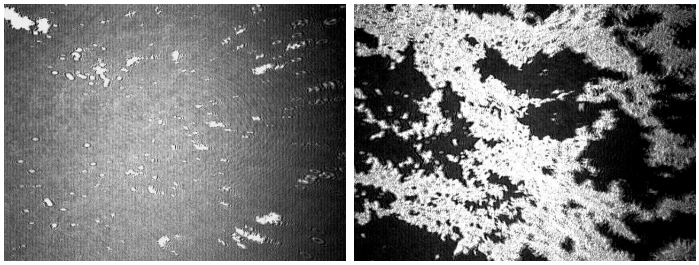

(d) A/M=36.9 Å^2 (e) A/M=23.9 Å^2

Figure 2.14: Brewster angle microscopy images of cholesteryl acetate. Figure(a) shows the coexistence of G + L_2 phase. The L_2 phase appeared with well defined boundaries. Figure(b) shows the G + L_2 phase coexistence. The L_2 phase appeared as mesh texture with voids. Figure(c) shows the predominant presence of L_2 phase with less G phase. Figure(d) shows the collapsed state of the L_2 phase to crystallites(bright spots). Figure(e) shows the growth of 3D crystallites. Each image has the dimension of 6.4 x 4.8 mm^2.

coexisting with G phase was seen even at large A/M(Figure 2.14(a)). With compression, L_2 phase was seen(Figure 2.14(b)). Further compression leads to predominant presence of L_2 phase (Figure 2.14(c)). In the collapsed state, bright crystallites were seen to grow from L_2 phase(Figure 2.14(d)). At still low A/M, big crystallites were seen(Figure 2.14(e)). These observations were consistent with our epifluorescence studies.

The BAM images of ChN are shown in Figure 2.15. The coexistence of G + bilayer phase is seen in BAM images(Figure 2.15(a)). We find that the bilayer phase was more fluid in nature. Interestingly, we find that this bilayer phase melts due to the heat generated by the probe laser itelf. This leads to the growth of G domains. This can be seen even during

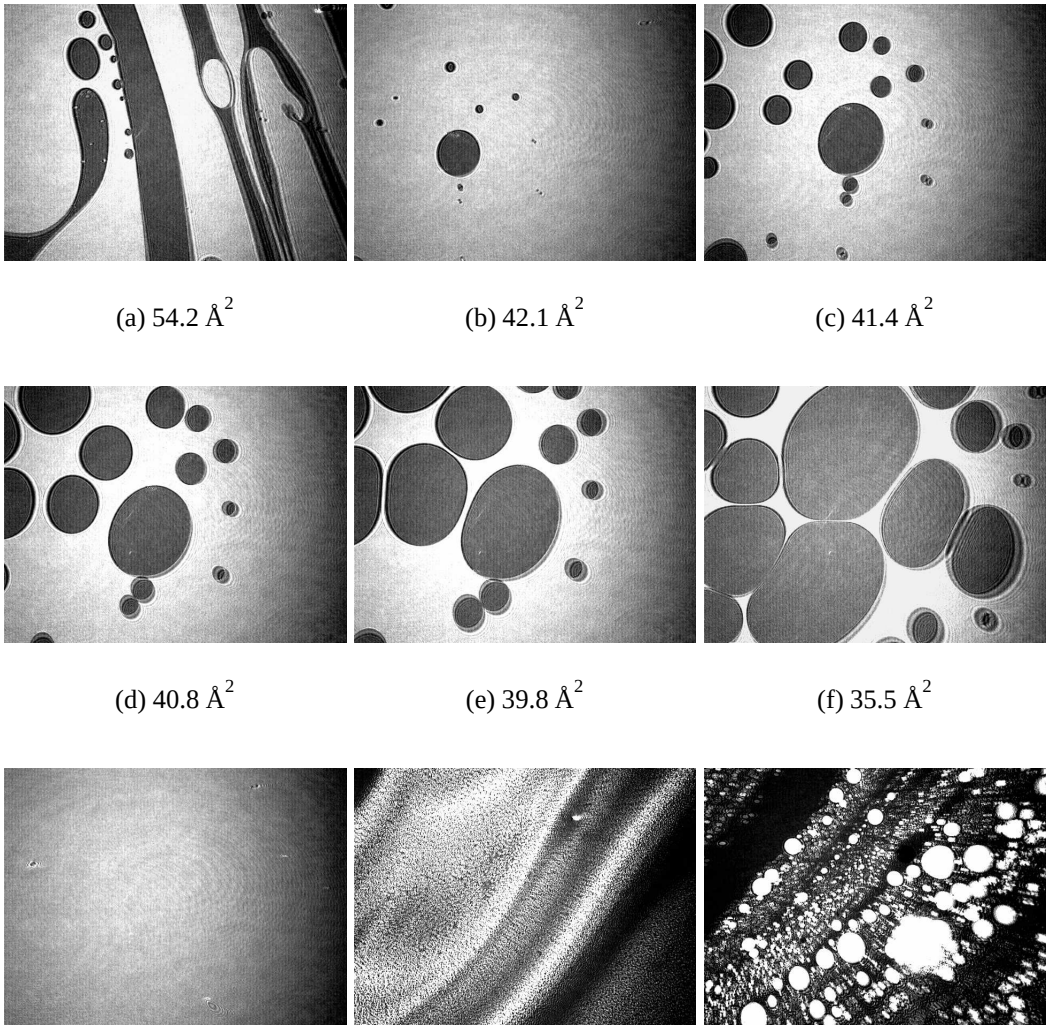

(a) 54.2 Å^2 (b) 42.1 Å^2 (c) 41.4 Å^2

(d) 40.8 Å^2 (e) 39.8 Å^2 (f) 35.5 Å^2

(g) 22.1 Å^2 (h) 12.7 Å^2 (i) 11.9 Å^2

Figure 2.15: Brewster angle microscopy images of cholesteryl nonanoate. Figure(a) shows the presence of coexisting gas(dark) and bilayer phase(bright background). Figures(b) to (f) show the growth of gas domains(dark) due to laser heating. Figure(g) shows the homogeneous and uniform bilayer phase. Figure(h) shows the collapsed state. Here the bright spots represent the 3D liquid domains. Figure(i) shows the collapsed state at lower A/M. Here bright spots coalesce to form bigger circles which tend to crystallize in time. Scale of each image is 6.4 x 4.8 mm^2.

compression, where in general one expects the G domains to decrease in size. This is shown in Figures 2.15(b) to 2.15(f). Figure 2.15(g) shows the presence of homogeneous bilayer phase. In the collapsed state, bilayer phase transformed to bright spots(Figure 2.15(h)). At still lower A/M, these bright spots coalesce to give larger circular domains which tend to crystallize in time(Figure 2.15(i)).

The BAM images of ChL are shown in Figure 2.16. At very large A/M, the G(dark) domains coexists with the background bilayer(bright) phase(Figure 2.16(a)). With compression, small circular bilayer(bright) and still brighter domains were seen to coexist with less G domains(Figure 2.16(b)). As in the case of ChN, we also observe the laser induced melting of the bilayer domains into G phase. This sequence is shown in Figures 2.16(c) to 2.16(e). At still lower A/M, the disordered structures were seen to develop(Figure 2.16(f)). For ChM,

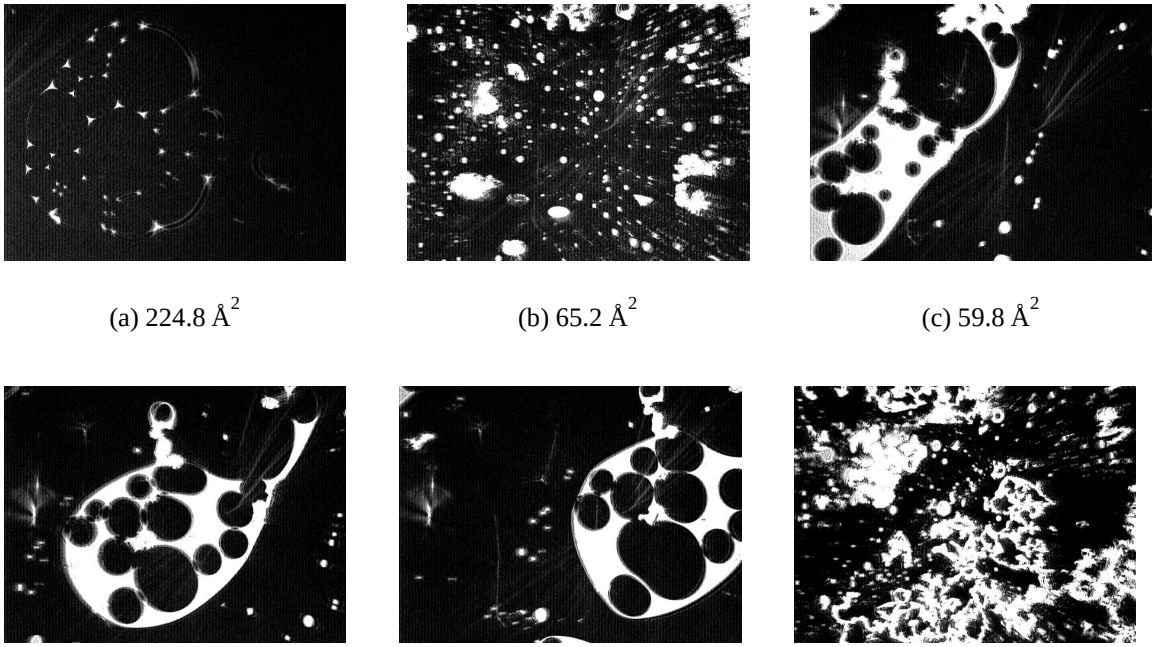

(a) 224.8 $Å^2$ (b) 65.2 $Å^2$ (c) 59.8 $Å^2$

(d) 59.8 $Å^2$ (e) 59.8 $Å^2$ (f) 53.7 $Å^2$

Figure 2.16: Brewster angle microscopy images of Cholesteryl Laurate. Figure(a) shows the G(dark) and bilayer (bright) coexisting phase. Figure(b) shows the appearance of still brighter domains which are thicker than the bilayer. These domains get distorted. Figures (c) to (e) shows the growth of gas(dark) domains due to laser heating. This shows the fluidity of the bilayer. Figure(f) shows the presence of irregular shaped structures. Scale of each image is 6.4 x 4.8 mm^2.

the BAM image indicates the presence of bright crystallites even at very high A/M. This is shown in Figure 2.17.

For the higher homologue of Ch derivatives like ChP and ChS the BAM textures appeared very similar. The images for ChP are shown in Figure 2.18. The texture showed bright network like structure with voids(dark)(Figures 2.18(a) and 2.18(b)). On compres-

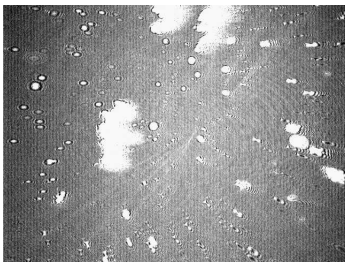

Figure 2.17: Brewster angle microscopy image of cholesteryl myristate. Figure shows the presence of bright irregular shaped 3D crystallites occurring at an A/M of 391 $Å^2$.

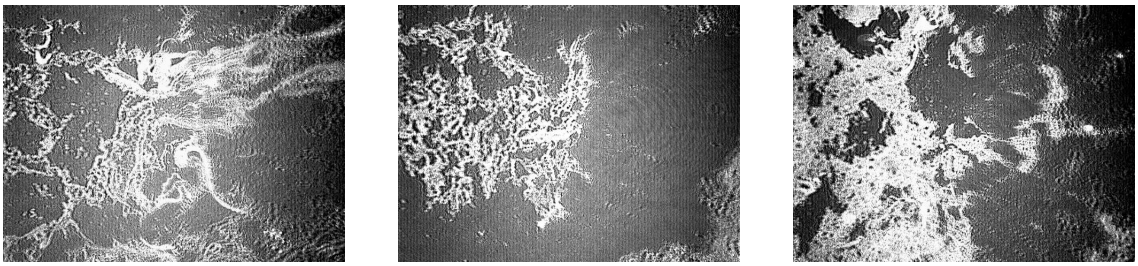

(a) 557.9 $Å^2$ (b) 348.7 $Å^2$ (c) 165.8 $Å^2$

Figure 2.18: Brewster angle microscopy images for cholesteryl palmitate. Figures (a) and (b) show the presence of highly irregular networks of disorder structures with voids(dark). Figure(c) shows the closely packed network structure with less voids. Scale of each image is 6.4 x 4.8 mm^2.

sion, the voids between the network decreased(Figure 2.18(c)). BAM images for ChS which are similar to that of ChP are shown in Figure 2.19.

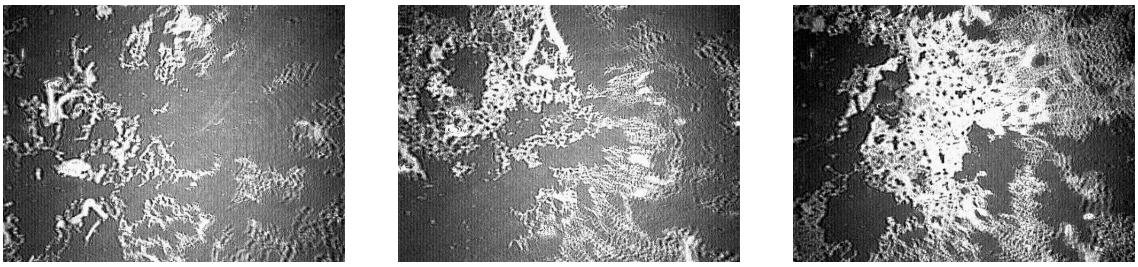

(a) 493 $Å^2$ (b) 221.3 $Å^2$ (c) 166 $Å^2$

Figure 2.19: Brewster angle microscopy images for cholesteryl stearate. Figures (a) and (b) show the presence of highly irregular networks of disorder structures. Figure(c) shows the closely packed network structure with less voids. Scale of each image is 6.4 x 4.8 mm^2.

For ChB, the BAM images are shown in Figure 2.20. Figures 2.20(a) and 2.20(b) show

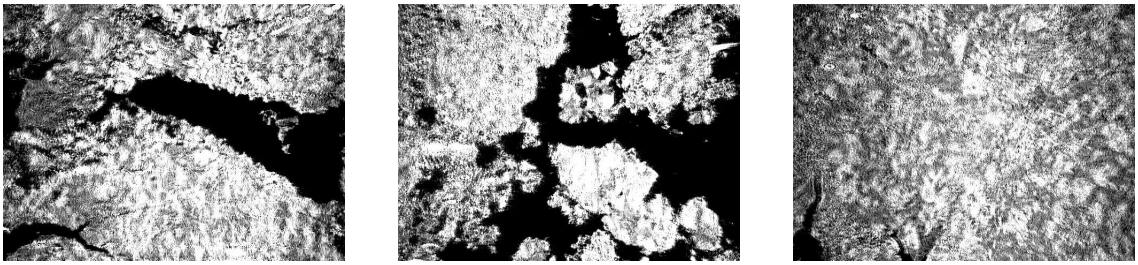

(a) 68 Å^2 (b) 46.8 Å^2 (c) 32.5 Å^2

Figure 2.20: Brewster angle microscopy images of cholesteryl benzoate. Figures (a) and (b) show the patterns having irregular sharp boundaries with voids. Figure(c) shows the presence of a crystalline pattern with less voids. Scale of each image is 6.4 x 4.8 mm^2.

the presence of crystalline bilayer phase with dark voids(G phase). The crystalline bilayer phase appeared bright with sharp and irregular boundaries. Upon compression, the voids between these structures were seen to decrease(Figure 2.20(c)). We also carried out the BAM studies with spreading solution of very low concentration(0.1 mM) to look for the usual G + L_2 coexistence phase. However, we found the textures to be the same. The BAM images for ChOl are shown in Figure 2.21. Figure 2.21(a) shows the predominantly present L_1 phase. Figures 2.21(b) and 2.21(c) show the collapsed state where L_1 phase and multilayer domains coexist. Initially the multilayer domains were small. With time, there was a progressive increase in the size of these multilayer domains(Figures 2.21(d) to 2.21(f)). The BAM textures for ChOC are shown in Figure 2.22. In Figure 2.22(a), the coexisting G + L_1(background) + bilayer(bright) phases were seen. The G domains tend to disappear upon compression leading to bilayer domains with L_1 phase in the background(Figures 2.22(b) and 2.22(c)). These bilayer domains coalesce and increase in size (Figures 2.22(d) to 2.22(f)). Figure 2.22(g) shows the collapse state. Here, the circular domains get distorted. Also, inside these domains brighter structures were seen. At still lower A/M, the boundaries of distorted circles vanished giving rise to more brighter structures(Figures 2.22(h) and 2.22(i)).

Reflection microscopy is a technique employed to image thicker films. For cholesteryl derivatives, we employed this technique to probe the textures at different A/M. This technique will provide information on the 3D domains after collapse. Our reflection microscopy

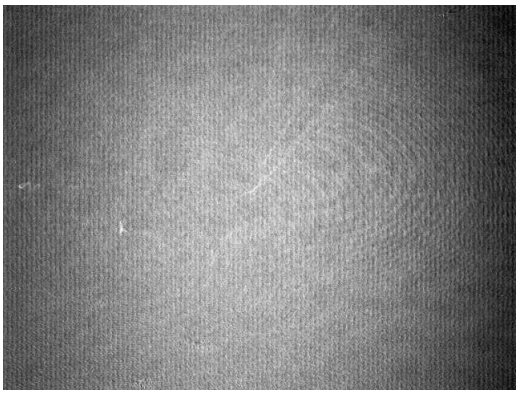

(a) 140.2 Å^2

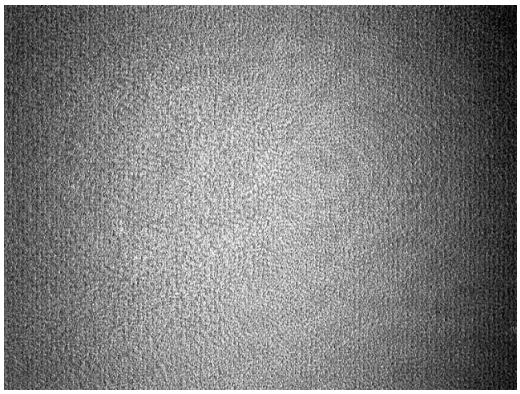

(b) 75.9 Å^2

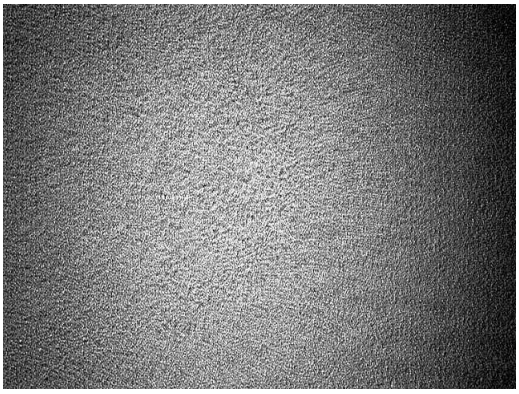

(c) 35.3 Å^2

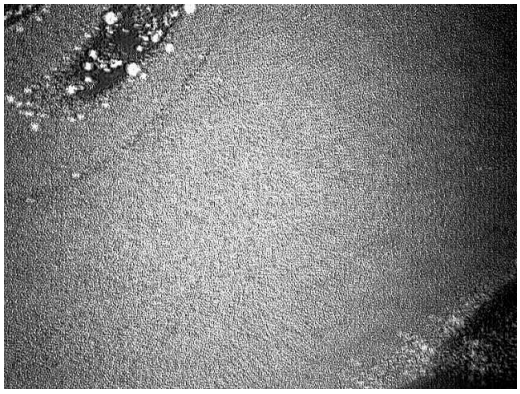

(d) 28 mins.

(e) 1hr 34 mins.

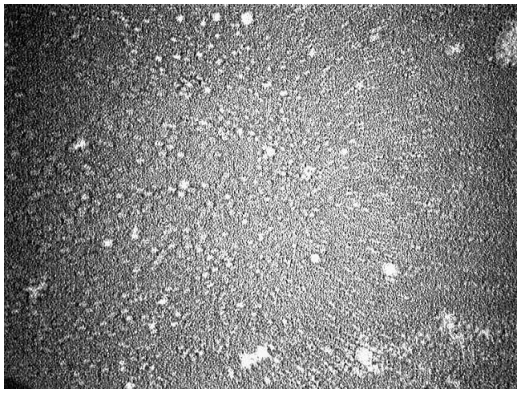

(f) 5hr 20 mins.

Figure 2.21: Brewster angle microscopy images for cholesteryl oleate. Figure(a) shows the predominant presence of L_1 phase. Figures (b) and (c) show the collapsed state. Here the small grainy domains represents multilayer phase. Figures (d) to (f) shows the increase in size of the multilayer domains with time. Scale of each image is 6.4 x 4.8 mm^2.

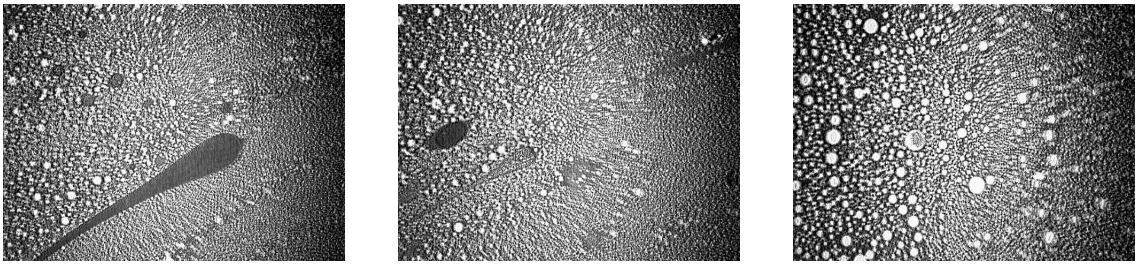

(a) 110.5 Å^2 (b) 88.8 Å^2 (c) 53.8 Å^2

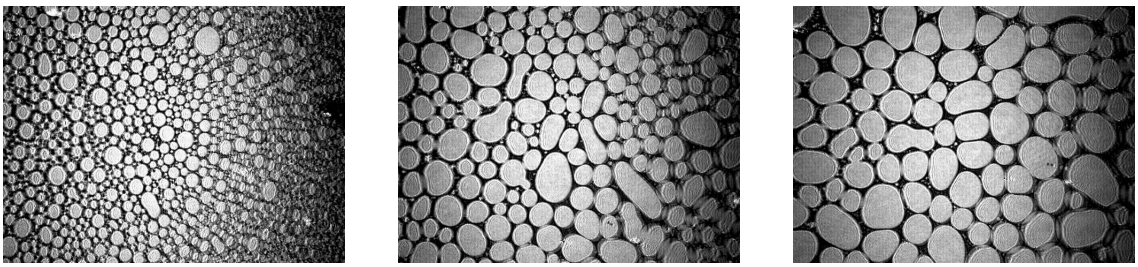

(d) 36.4 Å^2 (e) 32.0 Å^2 (f) 30.5 Å^2

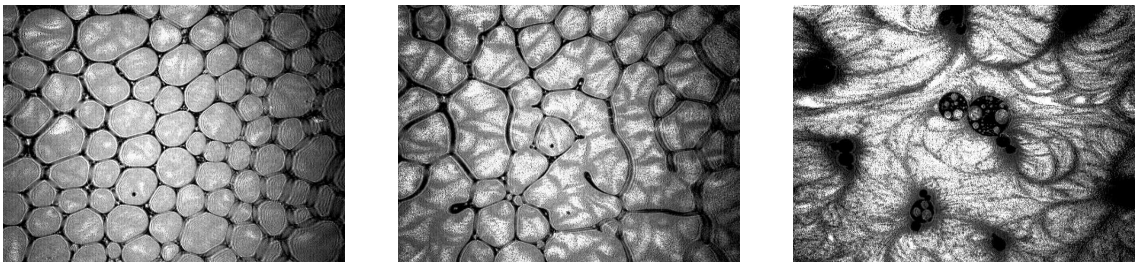

(g) 27.2 Å^2 (h) 25.9 Å^2 (i) 19 Å^2

Figure 2.22: Brewster angle microscopy images for cholesteryl oleyl carbonate. Figure(a) shows the coexisting gas(dark) domains along with L_1(background) and bilayer domains(bright spots). Figures (b) and (c) show the growth of bilayer phase in number and size with L_1 phase in the background. Figures (d) to (f) show the coalescing bilayer domains forming much bigger circular domains. Figures (g) and (h) show the presence of brighter structure within the bilayer domains. Figure(i) shows the much brighter structure within the bilayer phase. Scale of each image is 6.4 x 4.8 mm^2.

studies on ChH and ChO indicated the presence of 3D crystals immediately after spreading. For the case of ChN, in the collapsed state, we find the presence of small, circular and thicker domains. With time, these domains coalesce to form bigger circular domains which were brighter in the middle and less bright at the periphery(Figure 2.23(a)). These domains when left overnight, nucleate to give branched(Figure 2.23(b)) or dendritic pat-

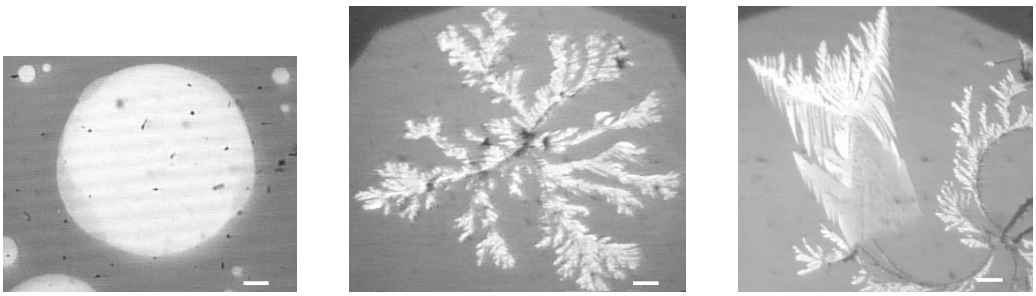

(a) 11.0 Å^2 (b) 11.0 Å^2 (c) 11.0 Å^2

Figure 2.23: Reflection microscope images of cholesteryl nonanoate in the collapsed state. Figure(a) represents the collapsed state with metastable domains. Here, the smaller bright droplets coalesce with time to grow into a bigger domain. These bigger domains are more intense in the center and weaker at the periphery. Figure(b) shows the evolution of the domain to branching patterns. Figure(c) shows the evolution to dendritic pattern. Scale bar represents 10 μm.

terns(Figure 2.23(c)). These were consistent with the textures seen under epifluorescence and BAM studies. The reflection microscopy images for ChL were similar to that of ChN. However, the thicker domains appeared in the low surface pressure region itself. These thicker domains which were fluid like(more mobile) fused into bigger domains. They transformed to crystallites at low A/M where the surface pressure was high. This indicated that the tendency to form crystals was more for ChL when compared to ChN.

For ChM, the reflection microscopy images indicated stiff sheet like textures even at very large A/M(Figures 2.24(a) to 2.24(c)). Over these flakes growth of a bright branched patterns were seen (Figures 2.24(a) to 2.24(c)). The textures obtained for ChP were very similar to that of ChM(Figure 2.25). At large A/M, bright branchy growths were seen over the stiff flake like structures. In the case of ChS, circularly shaped multilayer domains coexist with G phase (Figure 2.26(a)). Here the contrast was poor. Some of the multilayer domains were circular and others were deformed(Figure 2.26(b)). Here the fluidity was low indicating the crystalline nature. In the collapsed state, multilayer domains transformed to crumple pattern(Figure 2.26(c)). For the case of ChB, the onset of crystalline phase(dark spots) coexisting with bilayer phase is seen (Figure 2.27). With decrease A/M, more and more of 3D crystals(dark spots) are seen to coexist with bilayer phase(Figure 2.27(b)). For ChOl, in the

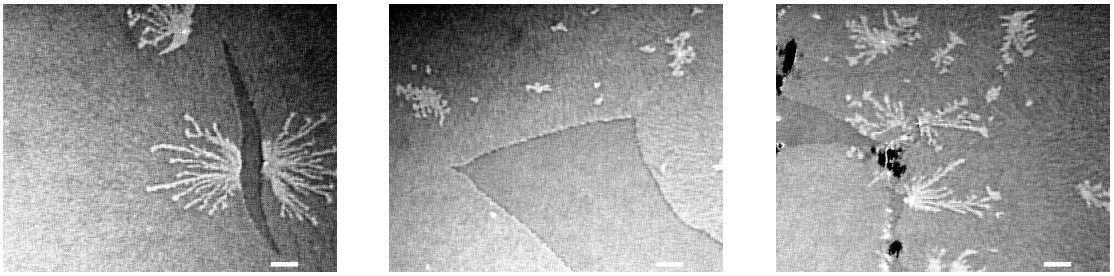

(a) 97.0 Å^2 (b) 91.5 Å^2 (c) 41.9 Å^2

Figure 2.24: Images of cholesteryl myristate under reflection microscope. Figure(a) shows the presence of fractures between the stiff thick flakes. Figures (a) and (b) show the occurrence of white branched growth of crystallites over the flakes. Figure(c) shows the presence of 3D crystallites(dark) which appear when the layers break down. Scale bar represents 10 μm.

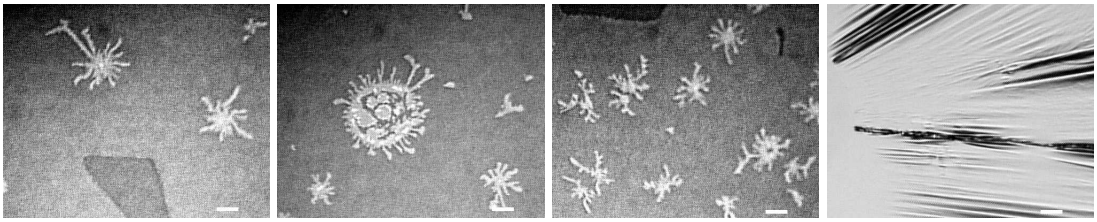

(a) 80.3 Å^2 (b) 70.9 Å^2 (c) 29.7 Å^2 (d) 13.9 Å^2

Figure 2.25: Images of cholesteryl palmitate under reflection microscope. Figures (a) to (c) show textures which are stiff thick flakes with fractures. Over the flakes white branched patterns are seen. At very low A/M, the flakes get crumpled and develop foldings. Scale bar represents 10 μm.

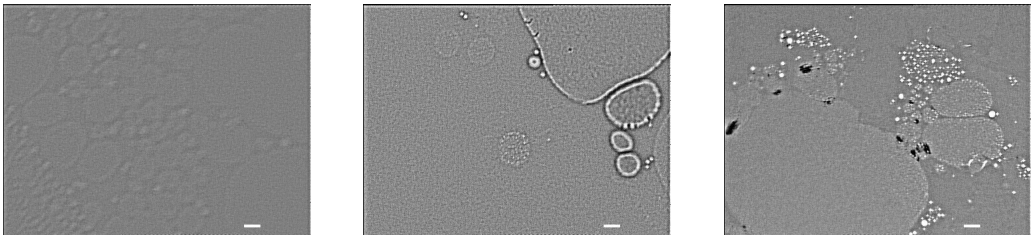

(a) 91.6 Å^2 (b) 59.7 Å^2 (c) 16.1 Å^2

Figure 2.26: Images of cholesteryl stearate under reflection microscope. Figure(a) shows the presence of circular multilayer domains. In Figure(b), these multilayer domains get distorted and coalesces into bigger domains. Figure(c) shows the crumpled pattern of the multilayer phase. Scale bar represents 10 μm.

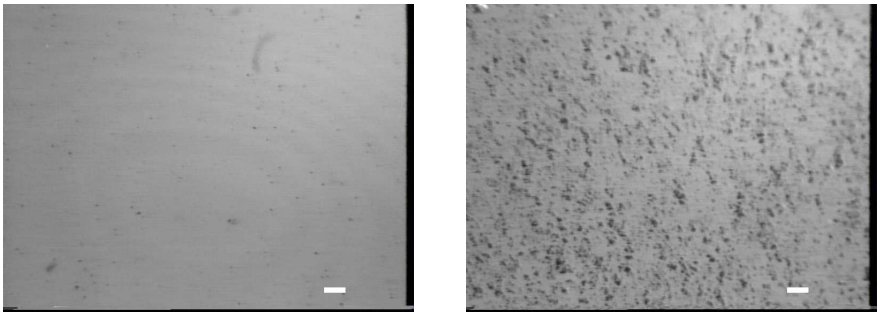

(a) 29 Å^2 (b) 23.4 Å^2

Figure 2.27: Images of cholesteryl benzoate under reflection microscope. Figure(a) shows the initiation of the nucleation process(dark spots) with coexisting crystalline bilayer phase as background. Figure(b) shows growth of crystallites(dark spots). Scale bar represents 10 μm.

collapsed state, initially the spots were randomly dispersed(Figure 2.28). initially the spots

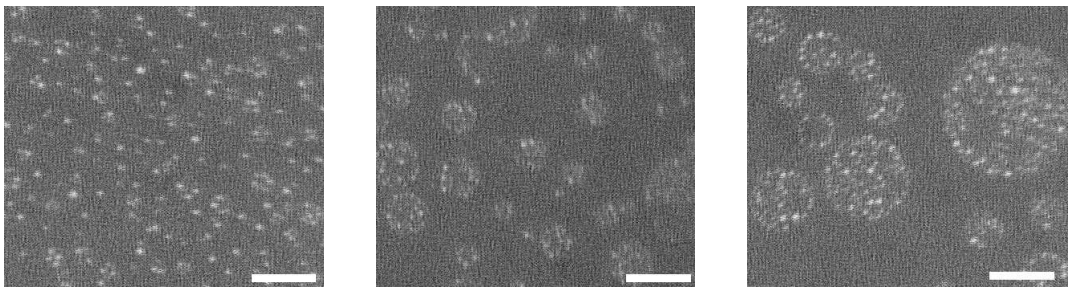

(a) 0 hour (b) 1 hour (c) 5 hour

Figure 2.28: Images of cholesteryl oleate in the collapsed state under reflection microscope. The images show the evolution of patterns with time. Figure(a) shows the appearance of small spots. Figures (b) and (c) show these spots arranging themselves within a circular domain. Scale bar represents 50 μm.

were randomly dispersed(Figure 2.28(a)). With time, these spots arranged themselves within a circular domain (Figures 2.28(b) and 2.28(c)). The reflection microscope studies on ChOC in the collapsed state show interference rings within the circular domains(Figure 2.29). This shows that the domains are lens shaped at the A-W interface.

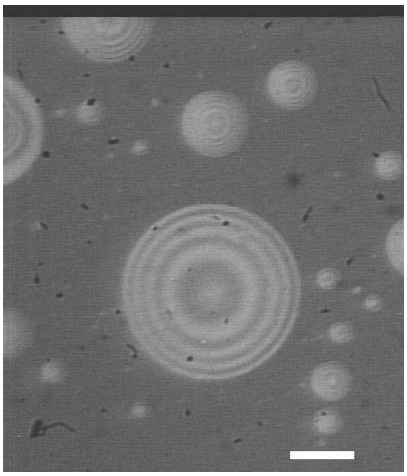

Figure 2.29: Images of cholesteryl oleyl carbonate under reflection microscope. The image shows the interference rings. This indicate that the domains are lens shaped. Scale bar represents 50 μm.

2.4 Discussions

The Ch molecules form a stable monolayer with very large collapse pressure(43.5 mN/m). From our epifluorescence and BAM studies, we find that above an A/M of 40 $Å^2$, the monolayer exhibited G + L_2 phase. The L_2 phase appeared less fluid. After the collapse, the L_2 phase continued to coexist with the 3D crystallites(Figures 2.3(b) and 2.13(c)). These observations are in agreement with other reports [14, 15]. For Ch, on depositing crystallites at A-W interface, ESP value of 38.1 mN/m was reached in about 10 minutes. This indicated that the molecules from the crystallites readily elute to form a monolayer. We also observed this process in-situ through BAM. This is in accordance with other reports [17]. For ChA, the trend in the isotherms and the limiting area per molecule, A_0 was almost the same as that of Ch. The collapse pressure value of ChA was 15.1 mN/m which was about one-third when compared to that of Ch. This reflects the weakly polar nature of ester group in ChA. Though the trend in the isotherm for ChA was similar to Ch, the microscopic textures were very much different. In ChA, under epifluorescence, a mesh texture was seen at large A/M(Figure 2.4(c)). This might be due to the higher crystalline nature of ChA monolayer due to the presence of ester group. This is in agreement with the recent grazing incident X-ray diffraction(GIXD) studies [5] which reveal a higher degree of crystallinity

in the monolayer phase. Our ESP experiments for ChA yielded value of 7.1 mN/m which is about half the value reported by Kwong et. al., [8]. However, in their case, excess ChA was added in the solution form which has an effect on the value of ESP. Also, our studies indicated that the kinetics to approach the ESP was quite longer for ChA(12 hours) when compared with Ch. We could observe the L_2 phase from the crystallites after elution under BAM. Dorfler and his co-workers have reported the isotherms for the short chain cholesteryl esters from acetate to butyrate [18]. Here, the decreasing trend in the collapse pressures with increase in alkyl chain length indicated the unstable monolayer behavior. Cadenhead and Philips [19] have reported that cholesteryl butyrate monolayer was unstable and yielded low collapse pressure of 7 mN/m with A_0 value of 42 $Å^2$. The unstable monolayer behavior has also been reported for cholesteryl caproate [19]. In the higher homologue like ChH and ChO, our studies show that they form unstable monolayer. The BAM and reflection microscopy studies indicated the formation of 3D crystals immediately after spreading. Our results are in accordance with the studies reported in the literature [19, 20]. Our studies showed that the higher homologue of esters after cholesteryl butyrate, viz., cholesteryl caproate, cholesteryl heptanoate and cholesteryl octanoate do not form stable monolayer and tend to crystallize upon spreading.

Interestingly, a different behavior was seen for ChN which is the immediate higher homologue. The isotherm indicated an A_0 value of 22 $Å^2$ which when compared to the estimated cross-section area of the molecule indicated a bilayer phase. The epifluorescence and BAM techniques reveal that this bilayer phase is more fluid and coexists with G phase(Figure 2.5(a) and 2.15(a)). In the BAM experiments for ChN, the heating caused by the probe laser melts the bilayer phase yielding G phase. Normally, one expects the G phase to decrease in area with compression. However, in this case, the effect was so dominant that the G phase continued to grow even during compression(Figures 2.15(b) to 2.15(f)). In the collapsed state, BAM and reflection microscopic techniques showed the occurrence of 3D drops which were in a metastable state(Figures 2.5(c) and 2.23(a)). These 3D metastable domains transformed to crystallites with branched and dendritic patterns(Figures 2.23(b)

and 2.23(c)) as seen under reflection. The higher homologue, ChL, yields low value of A_0 of 13.1 $Å^2$ which was not compatible with the molecular cross-section though it yields higher surface pressure compared to ChN. The bulk packing of ChL was reported to be of the type $m - i$ and also $m - ii$ [21]. Our studies on ChL indicated a higher tendency to nucleate and form crystals when compared to ChN. The epifluorescence studies indicate the presence of bilayer(bright) domains coexisting with G domains(Figure 2.6(a)). At low A/M, thicker and still bright domains were observed(Figures 2.6(b) to 2.6(d)). The BAM images indicate at very large A/M, fluidic bilayer domains coexisting with predominantly G phase(Figure 2.16(a)). With compression, the transformation of the bilayer domains to thicker domains were seen(Figures 2.16(b) to 2.16(e)). These thicker domains transform to crystallites(Figure 2.16(f)). This was also supported by our reflection microscopy studies. For cholesteryl tridecanoate, a crystalline bilayer behavior has been reported using surface manometry and GIXD technique [22]. Our investigations on the higher homologues like ChM, ChP and ChS reveal that the isotherms were quite similar with low A_0 and high surface pressure(65 mN/m) in agreement with the reported values [22]. Under epifluorescence, for ChM and ChP, flakes were seen with well defined edges. On top of these flakes, there were dark regions. These can be seen in Figures 2.7 and 2.8. Under reflection, the same dark regions appeared as white branchy textures(Figures 2.24 and 2.25). Under BAM, at very large A/M, for ChM, bright irregular textures were seen(Figure 2.17). For ChS, under epifluorescence, domains of varying intensity were seen(Figure 2.9). The jitters observed in the isotherms were due to these colliding crystallites. Under reflection, ChS films appeared as very faint circular domains(Figure 2.26(a)). Under BAM, the ChP and ChS films, at very high A/M, show similar irregular patterns(Figures 2.18 and 2.19). ChP and ChS were reported to form multilayers based on GIXD and ellipsometry techniques [22]. There are reports stating that the ChP and ChS form cloudy unstable films [7, 8]. Our observations indicate that though ChM, ChP and ChS gave rise to very high collapse pressure, the monolayer was unstable and forms sufficiently thick multilayers coexisting with 3D crystals.

According to Craven [21], the bulk packing of the cholesteryl derivatives has been clas-

sified broadly under three types(Figure 2.30) based on the interactions between the different parts of the molecules. They are the cholesteryl - cholesteryl(*m-i*), cholesteryl - chain(*m-*

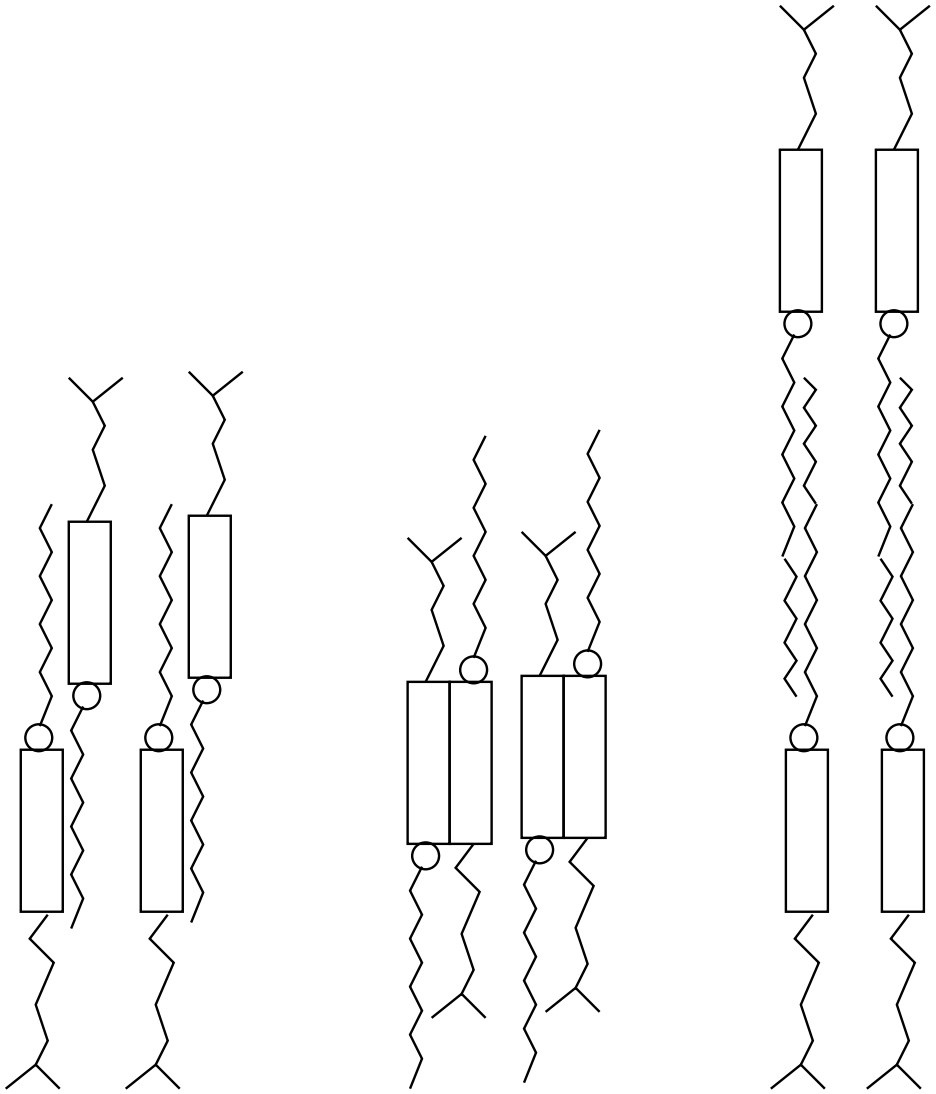

Figure 2.30: Classification of packing(represented schematically) for cholesteryl esters in bulk. Figures adapted from the reference [21]. Figure(a) represents the *m-ii* packing of cholesteryl esters from cholesteryl nonanoate to cholesteryl laurate. Figure(b) shows the *m-i* packing of the cholesteryl esters from cholesteryl caproate to cholesteryl octanoate. Figure(c) represents the *bilayer* packing of higher homologues of cholesteryl esters from cholesteryl tridecanoate onwards.

ii) and the chain - chain(*bilayer*) interactions. The short chain cholesteryl esters, from cholesteryl caproate to cholesteryl octanoate were classified as type *m-ii*(Figure 2.30(b)).

The other intermediate esters, cholesteryl nonanoate to cholesteryl laurate were classified as type *m-i*(Figure 2.30(a)) with the latter exhibiting both *m-i* and *m-ii* type packing. Still higher homologue of cholesteryl esters, cholesteryl tridecanoate onwards exhibit *bilayer*(Figure 2.30(c)) packing. For the case of unsaturated esters of cholesterol, both *m-i* and *m-ii* type packing have been observed.

Our studies on the cholesteryl derivatives show some correlation with the packing in bulk and the packing at the A-W interface. For the esters like ChH and ChO which belongs to *m-ii* type packing yielded 3D crystallites. Cholesteryl nonanoate in bulk come under the *m-i* packing(Figure 2.30(a)) as inferred by X-ray studies [21]. The lower homologue below ChN forms either cholesteric liquid crystalline phase or no mesophase at all. The higher members from ChN onwards exhibit the smectic phase in addition to cholesteric phase. Based on our studies on ChN and ChL behavior at the A-W interface, we speculate that the homologues which are intermediate may yield a bilayer phase at A-W interface.

For the higher homologues like cholesteryl tridecanoate, ChM, ChP and ChS, X-ray studies in bulk suggest *bilayer* packing [21]. Earlier monolayer study on cholesteryl tridecanoate at the A-W interface reported on the bilayer formation [22]. Based on our studies on some of the esters like ChM, ChP and ChS we expect that even in cholesteryl tridecanoate, 3D crystals coexist with the bilayer phase at the A-W interface. The minimum thickness of a domain which can be observed using reflection microscope is of the order of the wavelength of light(0.4 μm). If we assume that the thickness of bilayer to be around 40 Å, then the number of bilayers will be about 100. We have carried out our experiments for ChM, ChP and ChS even at low concentration(0.1 mM of $ChCl_3$) and also with a different solvent(Hexane). Even here, the crystallites can be observed under reflection indicating the absence of a stable monolayer in these materials.

In the case of ChB, we find a G + crystalline bilayer. It possessed a high collapse pressure of 60 mN/m and A_0 of 23.6 $Å^2$. The A_0 value corresponds to half of the cross-sectional area of ChB molecules suggesting the bilayer formation. We find that in the steep region of the ChB isotherm, when the compression is stopped keeping the A/M constant, the sur-

face pressure drops. This suggest that the bilayer phase was not stable. Our epifluorescence observations show that the dye does not disperse in the bilayer phase. BAM studies show patterns having irregular sharp boundaries with voids between them(Figure 2.20). Our reflection studies show the nucleation of crystallites(which appear dark) coexisting with bilayer phase(Figure 2.27). The unstable nature of the bilayer phase can be attributed to the growth of crystallites. Our studies contradict an earlier report on ChB which states the formation of a stable monolayer [23]. Further, our experiments of forming the monolayer on 2M NaCl subphase yielded same results for ChB. There are a few reports in the literature wherein the G + bilayer phases coexist [22], [24]. We find such a behavior for ChN, ChL and ChB systems. In the case of ChHC, the π-A/M isotherms are irreproducible. When it is studied under BAM and reflection microscopic techniques, the presence of crystallites were seen even at high A/M.

The unsaturated ester, ChOl, forms stable monolayer with the usual G + L_1 phase with a A_0 value of 114.4 $Å^2$. This is in agreement with the reports of Smawby and co-workers [25]. They conclude that the ester group within the subphase and the cholesteryl and alkyl chains in the air leads to this high value of A_0. Under epifluorescence, we find dense textures in the collapsed state(Figure 2.11(a)). With time, these textures transform to bright circular domains(Figures 2.11(b) to 2.11(d)). Our BAM observations(Figure 2.21) are in good agreement with epifluorescence observations. Under reflection microscope, in the collapsed state, we find randomly distributed bright domains(Figure 2.28(a)). With time, they arranged themselves within a big circular domain(Figures 2.28(b) and 2.28(c)). Studies on unsaturated esters, like cholesteryl linoleate, cholesteryl linolenate and cholesteryl arachidonate reported the deterioration of the monolayer with time due to oxidation [8]. Another derivative of Ch is cholesteryl oleyl carbonate which is a salt. The monolayer exhibited G + L_1 + bilayer coexisting phases. The A_0 value obtained from $\pi - A/M$ isotherm was not in conformity with the cross-sectional area of the molecule. This is likely to be due to the formation of bilayer. There is also another possibility that the material may dissolve in the subphase. It may also decompose. Under epifluorescence, ChOC exhibits G + L_1 + bilayer coexisting

phase(Figure 2.12(a)) which is followed by a uniform bilayer. In the collapsed state, bright domains coexist with bilayer phase(Figure 2.12(c)). Under compression, the bright domains arrange themselves in the periphery of larger domains(Figure 2.12(e)). These domains possess different intensities suggesting a variation in thickness. Under BAM, at very high A/M the presence of bright spots(bilayer) were seen along with G domains and L_1 phase in the background(Figures 2.22(a) and 2.22(b)). On compression, the bright bilayer domains increased in number and size(Figures 2.22(c) and 2.22(d)). They coalesce into bigger domains and get distorted(Figures 2.22(e) to 2.22(f)). Still bright structures were seen to grow within these bilayer domains(Figures 2.22(g) to 2.22(i)). ChOC forms cholesteric domains after collapse. Under reflection microscope, these showed interference rings indicating that they were lens shaped. Instead of the usual equilibration time of 10 minutes for the solvent evaporation, we have also studied with an equilibration time of 30 minutes. This showed an increase in the A_0 value of about 35 $Å^2$ indicating that ChOC may also decompose in time. The various phases of the cholesterol derivatives at the A-W interface are summarized in Table 2.1.

Table 2.1: Phases of cholesteryl derivatives at the air-water interface

Compounds	π_c(mN/m)	A_0(Å^2)	Surface phases
Ch	43.1	38.3	G + L_2, L_2, L_2 + crystallites
ChA	15.1	39.2	G + L_2, L_2, L_2 + crystallites
ChH, ChO	-	-	No monolayer formation (3D crystals)
ChN	2.4	22.0	G + bilayer, bilayer(fluid), bilayer + metastable domains (transforms to 3D crystals)
ChL	60	13.1	G + bilayer + multilayers + 3D crystals
ChM, ChP, ChS	≈65	19.6, 20.8, 21.1	G + multilayers + 3D crystals
ChB	65	23.7	G + bilayer(crystalline), bilayer + 3D crystals
ChHC	-	-	No monolayer formation (3D crystals)
ChOl	8	114.4	G + L_1, L_1, dense textures(transform to domains)
ChOC(salt)	3.4	28.7	G + L_1 + bilayer, L_1 + bilayer, bilayer + multilayers + cholesteric domains

We have undertaken a detail analysis on the structures and morphology of cholesteryl derivatives at the air-water interface using surface manometry, epifluorescence, BAM and reflection microscopy techniques. These results revealed the preferred hydrophobic interaction between the higher homologue of Ch which preferentially forms multilayers and crystallites at the A-W interface. The nature of packing of these multilayers have some correlation with the packing in bulk. The initial cholesteryl esters from cholesteryl formate to cholesteryl butyrate form monolayer. They become progressive unstable with lower value of collapse pressures. The other homologue like cholesteryl caproate, cholesteryl heptanoate and cholesteryl octanoate tend to form crystallites. Interestingly, for cholesteryl nonanoate we find that the bilayer phase at the air-water interface. These bilayers were more fluid. The still higher homologue cholesteryl laurate, which possess both m-i and m-ii type packing in the bulk, led to the formation of bilayer at very large A/M. But, the tendency to crystallize was more when compared to ChN. We speculate that the bilayer phases at air-water interface might continue to occur even for the homologues like cholesteryl decanoate and undecanoate which are in between cholesteryl nonanoate and cholesteryl laurate. For cholesteryl myristate, cholesteryl palmitate and cholesteryl stearate we find predominantly the formation of 3D crystals. Cholesteryl benzoate spontaneously form crystalline bilayer which transformed to crystallites at low A/M. In cholesteryl hydro cinnamate, the presence of flexible alkyl chain units destabilizes the monolayer and led to the formation of 3D crystals. The unsaturated ester, cholesteryl oleate tends to form a stable. The monolayer collapses to a dense state. This dense state evolves into 3D circular domains with time. Cholesteryl oleyl carbonate does not form a stable monolayer. Here, after the collapse, 3D circular domains appeared which arrange themselves in the periphery of less thicker domains.

Bibliography

[1] D.B. Zilversmit, Jour. Lip. Res., **180**, 9, 1968.

[2] T.G. Huang and A. Kuksis, Lipids, **2**, 443, 1967.

[3] B. Lundberg, Chem. Phys. Lip., **14**, 309, 1975.

[4] K. Simons and E. Ikonen, Science, **290**, 1721, 2001.

[5] H. Rapaport, I. Kuzmenko, S. Lafont, K. Kjaer, P. B. Howes, J. Als-Nielsen, M. Lahav and L. Leiserowitz, Biophy. Jour., **81**, 2729, 2001.

[6] S. Lafont, H. Rapaport, G.J. Somjen, A. Renault, P.B. Howes, K. Kjaer, J. Als-Nielsen, L. Leiserowitz and M. Lahav, J. Phys. Chem. B, **102**, 761, 1998.

[7] N.K. Adam and G. Jessop, Proc. Roy. Soc. (London) Ser. A., **120**, 473, 1928.

[8] C.N. Kwong, R.E. Heikkila and D.G. Cornwell, Jour. Lip. Res., **12**, 31, 1978.

[9] V. von Tscharner and H.M. McConnel, Biophys. Jour., **36**, 409, 1981.

[10] M. Losche, E. Sackmann and H. Mohwald, Ber. Bunsenges. Phys. Chem., **87**, 848, 1983.

[11] S. Henon and J. Meunier, Rev. Sci. Instr., **62**, 936, 1991.

[12] D. Honig and D. Mobius, J. Phys. Chem., **95**, 4590, 1991.

[13] R. Seoane, J. Minones, O. Conde, E. Iribarnegaray and M. Casas, Langmuir, **15**, 5567, 1999.

[14] R. Seoane, J. Minones, O. Conde, J. Minones Jr, M. Casas and E. Iribarnegaray, J. Phys. Chem. B, **104**, 7735, 2000.

[15] J.P. Slotte and P. Mattjus, Biochim. Biophys. Acta, **22**, 1254, 1995.

[16] S. Lafont, H. Rapaport, G. J. Somjen, A. Renault, P. B. Howes, K. Kjaer, J. Als-Nielsen, L. Leiserowitz and M. Lahav, J. Phys. Chem. B, **102**, 5, 1998.

[17] M. Iwahashi, A. Iwafuji, H. Minami, N. Katayama, K. Iimura and T. Kato, Mol. Crys. Liq. Crys., **337**, 117, 1999.

[18] H.D. Dorfler and W. Rettig, Coll. Poly. Sci., **260**, 802, 1982.

[19] D. A. Cadenhead and M. C. Philips, Jour. of Coll. Int. Sci., **24**, 491, 1967.

[20] J.M. Smawby and H.L. Brockman, Biochemistry, **20**, 724, 1971.

[21] B.M. Craven, *Handbook of Lipid Research, The physical chemistry of lipids*, Edited by D. M. Small, Plenum press:NY, 1986.

[22] C. Alonso, I. Kuzmenko, T.R. Jensen, K. Kjaer, M. Lahav and L. Leiserowitz, J. Phys. Chem. B, **105**, 8563, 2001.

[23] S. Mukherjee, R. Chatterjee and S.K. Bose, Chem. Phys. Lip., **23**, 85, 1978.

[24] N.L. Gershfeld and K. Tajima, Nature, **279**, 708, 1979,

[25] J.M. Smawby and H.L. Brockman, Biochemistry, **23**, 3312, 1984.